Sensitivity of Vehicle System Vibrations to Subsystem Structural Variations

(Received: January 26, 2012. Revised: July 18, 2012. Accepted: August 28, 2012)

M. Karpel[1]
V. R. Feldgun[2]
B. Moulin[3]

Abstract
The fictitious-mass modal coupling method is extended to include sensitivity analysis of system-level performance to parametric changes in sub-system structural properties. With fictitious masses loading the interface coordinates, the sub-system normal modes can serve as a fixed set of generalized coordinates. The resulting model is very efficient and of high-accuracy. The extended method is demonstrated by the evaluation of deterministic and stochastic acceleration response parameters of a typical vehicle traveling over a rough road, and their derivatives with respect to local structural variations. The vehicle is divided into several structural components represented by separate normal modes produced with fictitious masses loading their interface coordinates. The examined variables are stiffness and damping values of component interconnection elements, and natural frequencies of the separate components.

1. Introduction

Vibration analysis of vehicle structures require the construction of detailed finite element models for the various subsystems, and their assembly for the finite-element model of the entire vehicle that typically have hundreds of thousands degrees of freedom. To allow reasonable computation in repeated analyses during the design process, structural dynamic analyses are performed by using the modal approach where the displacement vector is assumed to be a linear combination of a relatively small set of low-frequency natural vibration modes (typically less than one hundred modes). Numerical efficiency in repeated dynamic analyses where parametric variations are made in the structural properties of one subsystem while the other subsystems remain unchanged calls for the use of component mode synthesis (CMS) where modal properties of several substructures are coupled for the generalized equations of motion of the entire structure.

A comparative overview of some of the leading CMS methods is given in Ref. [1], where CMS methods are classified according to the interface boundary conditions of the component normal modes. The classification types are fixed-interface modes, free-interface modes and loaded-interface modes. Hurty [2] and Craig and Bampton [3] based their fixed-interface formulations on the assumption that the motion of each component, as part of the entire structure, is a linear combination of two sets of isolated component modes: 1) a number of low-frequency fixed-boundary natural vibration modes, and 2) all the static constraint modes obtained by imposing a unit displacement on one of the boundary coordinates, while holding the remaining boundary coordinates fixed. The resulting model contains the necessary near-boundary structural information, but it might become inefficient when the number of boundary coordinates is large. It might also be difficult to apply with standard finite-element codes because it is based on two different analyses, static and dynamic. Other disadvantages of the CB method are that the resulting model may contain very high natural frequencies that might cause numerical difficulties in dynamic simulations, and that it can not be applied with component modes obtained from vibration tests.

[1] Professor, Faculty of Aerospace Engineering. Technion, Israel Institute of Technology.
[2] Senior Researcher, Faculty of Civil and Environmental Engineering.
[3] Formerly Senior Researcher, Faculty of Aerospace Engineering.

doi:10.3293/asdj.2012.18

A different approach, which requires only one set of modes with free boundary coordinates, was taken by Goldman [4] and by Hou [5]. These methods were more convenient because they used natural vibration modes only. However, with the boundary points unloaded, vital information about the structural deformations near the boundary is not included in the component modes, which leads to inaccuracies and slow convergence with the number of component modes. Benfield and Hruda [6] loaded the free boundary coordinated with reduced stiffness and mass matrices of the neighboring substructures, and MacNeal [7] and Rubin [8] added static attachment modes which are based on static responses to loads at each interface coordinate. These modifications improved the free-coordinate results but are more difficult to apply because of the added static modes, and might be less efficient in modular, multi-configuration cases.

A previous paper in the presented research program [9] dealt with a CMS procedure that uses fictitious masses [10] to load the interface coordinated when the normal modes of the separate components are calculated. Ref. [9] extended previous fictitious-mass techniques [11, 12] to allow three types of interface connections: rigid, soft and structural links. While rigid connections imply displacement compatibility across the interface, soft connections introduce interface springs. The structural links have their own typically small finite-element models that retain their discrete coordinates in the coupling equations. The coupled equations of motion were applied in Ref. [9] to calculations of dynamic response of a vehicle to random road excitation. Major advantages of the fictitious-mass technique are that: a) the component boundary conditions in the separate normal modes analyses are closer to the actual ones, in the assembled structure, than unloaded or clamped boundaries used in other coupling methods; and b) it is very effective and robust when used in conjunction with component vibration tests [13, 14].

The development process of a vehicle system includes the assignment of requirements for the structural design of the separate subsystems and the interconnection elements to assure favorable system-level vibration performance. The requirements can be defined in terms of limits on stiffness, mass and damping properties of discrete elements and/or in terms of modal properties, such as certain component natural frequencies, that can be verified in vibration tests. To facilitate an effective establishment of design requirements and an efficient evaluation of the effects of parametric changes and manufacturing deviations on system-level performances, it is desired to develop an efficient computational tool for calculating the sensitivity derivatives of performance parameters with respect to component structural parameters and natural frequencies. The purpose of the work presented in this paper was to extend the modal coupling technique of Ref. [9] for calculating such derivatives, and to apply the extended technique to a benchmark vehicle model.

2. Frequency Response by Modal Coupling

Modal frequency response analysis to an excitation force vector $\{F(i\omega)\}$ associated with a unit-amplitude input can be performed by solving

$$[W(i\omega)]\{\xi(i\omega)\} = [\phi]^T \{F(i\omega)\} \tag{1}$$

where $[f]$ is the matrix of normal modes taken into account, and

$$[K_E] = [\phi]^T [K_G] [\phi] \tag{2}$$

Where

$$[K_G] = \left(\sum_j G_{E_j} [K_{E_j}] \right) \tag{3}$$

where $\left[K_{E_j}\right]$ is the stiffness matrix of an element to which a structural damping coefficient G_{E_j} is assigned. The modal viscous damping matrix can be calculated by

$$[B] = [\phi]^T [B_D] [\phi] \tag{4}$$

where $[B_D]$ is the discrete-coordinate viscous damping matrix due to viscous elements. Alternatively, it is often assumed to be diagonal with given modal damping parameters (see below). The structural matrices in Eq. (1) can accommodate all the linear structural modeling options in MSC/NASTRAN, which uses the normal modes of the entire structural system as generalized coordinates. The structural matrices $[M]$ and $[K]$ in Eq. (1) are diagonal in this case, but the modal damping matrices in Eq. (1) are generally not diagonal. With this approach, specific structural components and interconnection links cannot be represented explicitly in the model, and local structural variations usually require repeated analyses with the entire model. When CMS is used, $[M]$ and $[K]$ become non diagonal, but the reduced-size model can be constructed such that high-accuracy analyses with local structural variations can be performed efficiently without returning to the full finite-element model.

The coupling method of Ref. [9] facilitates the coupling of several structural components interconnected by structural links. The matrices in Eq. (1) are constructed from the component modes and the interface elements. For the sake of simplicity, the formulation below assumes two components, A and B, and one interface link. The generalized displacement vector $\{\xi\}$ of Eq. (1) is composed in this case of $\{\xi_A\}$, $\{\xi_B\}$ and $\{u_S\}$, where $\{\xi_A\}$ and $\{\xi_B\}$ are the modal displacements with respect to the separate component modes, and $\{u_S\}$ is the vector of discrete displacements of the structural link. The coupling process is based on the assumption that the discrete displacements of the coupled system are, at all times, linear combinations of the separate modes and the structural links,

$$\{u(t)\} = [\phi] \{\xi(t)\} \tag{5}$$

Where

$$\{u\} = \begin{Bmatrix} u_A \\ u_{IA} \\ u_B \\ u_{IB} \\ u_S \end{Bmatrix}, \quad [\phi] \begin{bmatrix} \phi_A & & \\ \phi_{IA} & & \\ & \phi_B & \\ & \phi_{IB} & \\ & & I \end{bmatrix}, \quad \{\xi\} = \begin{Bmatrix} \xi_A \\ \xi_B \\ u_S \end{Bmatrix} \tag{6}$$

where the subscripts IA and IB denote the interface of A and the interface of B correspondingly, $[f_A]$ and $[f_B]$ are the normal modes of components A and B, calculated with fictitious masses $[M_{FA}]$ and $[M_{FB}]$ loading their interfaces to the structural link model; $[f_{IA}]$ and $[f_{IB}]$ are matrices of the modal displacements at the interface coordinates of the structural components. As developed in Ref. [9], the coupled undamped free-vibration equation of motion in this case is

$$\begin{bmatrix} M_A + M_{IA} & M_{AB} & M_{AS} \\ M_{AB}^T & M_B + M_{IB} & M_{BS} \\ M_{AS}^T & M_{AS}^T & M_{SS}^{(1)} \end{bmatrix} \begin{Bmatrix} \ddot{\xi}_A \\ \ddot{\xi}_B \\ \ddot{u}_S^{(1)} \end{Bmatrix} + \begin{bmatrix} \Omega_A M_A + K_{IA} & K_{AB} & K_{AS} \\ K_{AB}^T & \Omega_B M_B + K_{IB} & K_{BS} \\ K_{AB}^T & K_{BS}^T & K_{SS}^{(1)} \end{bmatrix} \begin{Bmatrix} \xi_A \\ \xi_B \\ u_S^{(1)} \end{Bmatrix} = \{0\} \tag{7}$$

Where $[M_A]$, $[M_B]$, $[\Omega_A M_A]$ and $[\Omega_B M_B]$ are the mass and stiffness matrices of the separate components, where $[\Omega_A]$ and $[\Omega_B]$ are diagonal matrices with the respective eigenvalues, namely the squared values of the respective natural

frequencies. The other matrices in Eq. (5) are

$$\begin{bmatrix} M_{IA} & M_{AB} & M_{AS} \\ M_{AB}^T & M_{IB} & M_{BS} \\ M_{AS}^T & M_{BS}^T & M_{SS}^{(1)} \end{bmatrix} = \begin{bmatrix} \varphi_{IA}^T \left(M_{AA}^{(1)} - M_{FA} \right) \varphi_{IA} & \varphi_{IA}^T M_{AB}^{(1)} \varphi_{IB} & \varphi_{IA}^T M_{AS}^{(1)} \\ & \varphi_{IB}^T \left(M_{BB}^{(1)} - M_{FB} \right) \varphi_{IB} & \varphi_{IB}^T M_{BS}^{(1)} \\ Sym & & M_{SS}^{(1)} \end{bmatrix};$$
$$\begin{bmatrix} K_{IA} & K_{AB} & K_{AS} \\ K_{AB}^T & K_{IB} & K_{BS} \\ K_{AS}^T & K_{BS}^T & K_{SS}^{(1)} \end{bmatrix} = \begin{bmatrix} \varphi_{IA}^T K_{AA}^{(1)} \varphi_{IA} & \varphi_{IA}^T K_{AB}^{(1)} \varphi_{IB} & \varphi_{IA}^T K_{AS}^{(1)} \\ & \varphi_{IB}^T K_{BB}^{(1)} \varphi_{IB} & \varphi_{IB}^T K_{BS}^{(1)} \\ Sym & & K_{SS}^{(1)} \end{bmatrix} \tag{8}$$

where the matrices with the superscript (1) are partitions of the discrete-coordinate mass and stiffness matrices with subscripts A, B and S relating to component A, component B and the structural link between them. It should be noticed that the structural link may have no inner degrees of freedom, which implies an empty $\{u_S\}$ vector and the elimination of the associated partitions in Eqs. (6) and (7). However, the direct interconnection matrices between components A and B may still exist similarly to those of direct "soft" connections. Frequency response analysis via modal coupling is performed by solving Eq. (1) with $\{\xi\}$ replaced by the displacement vector of Eq. (5), and the generalized mass and stiffness matrices by those of Eq. (5). The other matrices in $[W(i\omega)]$ of Eq. (1) are

$$[B] = \begin{bmatrix} B_A + \phi_{IA}^T B_{AA}^{(1)} \phi_{IB} & \phi_{IA}^T B_{AB}^{(1)} \phi_{IB} & \phi_{IA}^T B_{AS}^{(1)} \\ & B_B + \phi_{IA}^T B_{BB}^{(1)} \phi_{IB} & \phi_{IB}^T B_{BS}^{(1)} \\ Sym & & B_{SS}^{(1)} \end{bmatrix}; \tag{9}$$

$$[K_E] = \begin{bmatrix} K_{E_A} \phi_A^T K_{G_{AA}}^{(1)} \phi_B & \phi_A^T K_{G_{AB}}^{(1)} \phi_B & \phi_{IA}^T K_{G_{AS}}^{(1)} \\ & K_{E_B} + \phi_A^T K_{G_{BB}}^{(1)} \phi_B & \phi_{IB}^T K_{G_{BS}}^{(1)} \\ Sym & & K_{G_{SS}}^{(1)} \end{bmatrix}; \tag{10}$$

where the matrices with the superscript (1) are partitions of the discrete-coordinate viscous-damping and structural-damping matrices, similarly to the mass and stiffness terms in Eq. (6). The component modal damping matrices are usually defined by modal damping parameters, for example

$$[B_A] = 2\,[\xi_A]\,[M_A]\,[\omega_A] \tag{11}$$

where $[\xi_A]$ and $[\omega_A]$ are diagonal matrices of the associated modal damping and natural frequency values. The right hand side of Eq. (1) becomes

$$\{F_i(i\omega)\} = [\phi]^T \{F_i(i\omega)\} = \begin{Bmatrix} \phi_A^T F_A(i\omega) \\ \phi_B^T F_B(i\omega) \\ F_S^{(1)}(i\omega) \end{Bmatrix} [M_A]\,[\omega_A] \tag{12}$$

Equation (1) with the coupled modal matrices of Eqs. (5) to (9) can be used directly for dynamic response analysis. Alternatively, one can use Eq. (5) for calculating the coupled normal modes and then use them to diagonalize $[M]$ and $[K]$, as detailed in Ref. [9]. The eigenvalues $[\Omega_H]$ and eigenvectors $[\Psi_H]$, normalized to unit generalized mass, obtained by the normal modes analysis based on Eq. (5) are used in the diagonalization process. By the substitution

$$\{\xi\} = [\Psi_H]\,\{\xi_{new}\} \tag{13}$$

in Eq. (1) and pre-multiplication by $[\Psi_H]^T$, a matrix equation of motion is obtained for $\{\xi_{new}(i\omega)\}$ where the mass and stiffness matrices are diagonal. The main advantage of this system is that each modal coordinate is related now to a specific natural frequency and mode shape. If, for example, one is interested in frequency response in a certain range, the modal coordinates associated with higher frequencies would be truncated. The truncation is done by eliminating unimportant columns from $[\Psi_H]$, which results in a lower-order system matrix $[W]$ in Eq. (1). The frequency response vector $\{\xi(i\omega)\}$ can be used for calculating the discrete displacement, velocity and acceleration response vectors by using Eq. (4),

$$\begin{aligned} \{H_d(i\omega)\} &= [\phi]\{\xi(i\omega)\} \\ \{H_v(i\omega)\} &= i\omega[\phi]\{\xi(i\omega)\} \\ \{H_a(i\omega)\} &= -\omega^2[\phi]\{\xi(i\omega)\} \end{aligned} \tag{14}$$

When the system is diagonalized before calculating the frequency response, Eq. (11) becomes

$$\begin{aligned} \{H_d(i\omega)\} &= [\phi_{new}]\{\xi_{new}(i\omega)\} \\ \{H_v(i\omega)\} &= i\omega[\phi_{new}]\{\xi_{new}(i\omega)\} \\ \{H_a(i\omega)\} &= -\omega^2[\phi_{new}]\{\xi_{new}(i\omega)\} \end{aligned} \tag{15}$$

where $[\phi_{new}] = [\phi][\Psi_H]$

When the direct approach is taken via Eq. (11), the response at a certain location depends on the modes of the respective component only, as indicated by Eq. (4), but it is important to consider all the component modes taken into account in the coupling equations. When the new-basis approach is taken through Eq. (12), each mode contains displacements of all the model points. However, high-frequency modes may be truncated without having significant effects on the recovered discrete response values.

3. Sensitivity of Frequency Response to Structural Changes

The derivatives of frequency response parameters to structural changes are defined by the derivatives of the response parameters of Eq. (11) with respect to the changed properties,

$$\begin{aligned} \frac{\partial\{H_d(i\omega)\}}{\partial p} &= [\phi]\frac{\partial\{\xi(i\omega)\}}{\partial p} \\ \frac{\partial\{H_v(i\omega)\}}{\partial p} &= i\omega[\phi]\frac{\partial\{\xi(i\omega)\}}{\partial p} \\ \frac{\partial\{H_a(i\omega)\}}{\partial p} &= -\omega^2[\phi]\frac{\partial\{\xi(i\omega)\}}{\partial p} \end{aligned} \tag{16}$$

where $[f]$ is not differentiated because it is a matrix of fixed modal coordinates not to be confused with the actual normal modes of the structure. Hence, the use of Eq. (11) for sensitivity analysis is preferred over Eq. (12) that would require the differentiation of $[f_{new}]$. The derivatives of the modal response vector in Eq. (13) is obtained by the differentiation of Eq. (1) which yields

$$\begin{aligned} \frac{\partial\{\xi(i\omega)\}}{\partial p} &= \frac{\partial\left[W(i\omega)^{-1}\right]}{\partial p}[\phi]^T\{F(i\omega)\} \\ &= [W(i\omega)]^{-1}\frac{\partial[W(i\omega)]}{\partial p}[W(i\omega)]^{-1}[\phi]^T\{F(i\omega)\} \end{aligned} \tag{17}$$

The modal-coupling formulation described in the previous section offers significant advantages when used for sensitivity analysis. Since a specific structural change is associated with a specific substructure or a specific structural link, the resulting sensitivity matrix $\partial [W(i\omega)] / \partial p$ would be mostly zero, except for the relevant partitions. A major question is, of course, whether the CMS approach is sufficiently accurate for sensitivity analysis. The answer is that the use of fictitious masses at the interfaces of the separate components while their modes are generated, can provide the required accuracy, as will be demonstrated by the numerical applications below.

Two practical sensitivity cases are formulated and demonstrated in this paper: (a) derivatives with respect to natural frequencies of separate substructures, which can be instrumental in defining design and acceptance criteria to component developers; and (b) derivatives with respect to discrete properties of structural links that may be used in their design process.

The only parts of $[W]$ that are functions of the component natural frequencies are the stiffness matrix of Eq. (5) and the damping matrix in Eq. (8). The derivatives of these matrices are zero matrices except for a single non-zero element in each matrix. For example, the non-zero terms in $\partial [W(i\omega)] / \partial p$ with respect to the first natural frequency of substructure A are

$$\frac{\partial K_{11}}{\partial \omega_{A_1}} = 2 M_{A_{11}} \omega_{A_1} \tag{18}$$

and, when Eq. (8) is used

$$\frac{\partial B_{11}}{\partial \omega_{A_1}} = 2 M_{A_{11}} \varsigma_{A_1} \tag{19}$$

The derivatives in Eqs. (15) and (16) are with respect to the natural frequencies of the components calculated with boundary fictitious masses. If one wants to calculate the derivatives with respect to natural frequencies associated with a different set of fictitious masses, including no fictitious masses at all, the component modes should be first transformed to a new set of modes. The transformation can be performed by applying the component diagonalization process described in Ref. [9], where the difference between the two sets of fictitious boundary masses is removed. Once the transformation is performed, the fictitious mass matrices in Eq. (6) become the new ones and the eigenvalues in Eq. (5) are those associated with the new fictitious masses.

The derivatives of $[W]$ with respect to changes in structural links are defined by the derivatives of the structural matrices in Eqs. (6-8). For example, the derivatives with respect to a structural parameter that affects Link #1 are

$$\frac{\partial [W(i\omega)]}{\partial p} =$$

$$\left[\phi^{(1)}\right]^T \left(-\omega^2 \frac{\partial \left[M^{(1)}\right]}{\partial p} + i\omega \frac{\partial \left[B^{(1)}\right]}{\partial p} + (1 + iG) \frac{\partial \left[K^{(1)}\right]}{\partial p} + i \frac{\partial \left[K_G^{(1)}\right]}{\partial p} \right) \left[\phi^{(1)}\right] \tag{20}$$

where

$$\left[\phi^{(1)}\right] = \begin{bmatrix} \phi_{IA} & & \\ & \phi_{IB} & \\ & & I \end{bmatrix} \tag{21}$$

The derivatives of $[W]$ are used for calculating the derivatives of the frequency response of the modal displacements, Eq. (14), and then the frequency response of the selected displacements, velocities and accelerations, Eq. (13).

4. Response to Random Road Excitation

The formulation of random response analysis to road excitation in this paper is identical to that of Ref. [9] , except that a time delay is now defined between the front and rear tires. The bottom points of the tires are loaded by large masses of 10^6 tons each in the z coordinate. The application forces that are equal to the prescribed accelerations times the large added masses enforce the required excitation accelerations. The input accelerations imposed by a rough road are defined in statistical terms by the acceleration Power Spectral Density (PSD) functions $S_{11}(\omega)$ and $S_{22}(\omega)$ of the inputs to the right and left wheels, and the complex cross correlation function $S_{12}(i\omega)$.

Random response is based on frequency response parameters to separate right- and left- wheel excitations. In each case, the force vector $\{F(i\omega)\}$ in Eq. (1) is zero, except for

$$F_{front} = 10^6 \quad ; \quad F_{rear} = 10^6 e^{-i\omega\tau} \tag{22}$$

where t is the time delay between the two wheels. These forces are applied at the wheel bottom points, in the z direction, where the large masses were added. The solution of Eq. (1), $\{\xi(i\omega)\}$, is used in each case for calculating the frequency responses $H_1(i\omega)$ and $H_2(i\omega)$ of a desired parameter to right and left excitations. These are used for calculating the PSD of the output parameter in response to a simultaneous excitation

$$S_{out}(i\omega) = \begin{bmatrix} H_1(i\omega) & H_2(i\omega) \end{bmatrix} \begin{bmatrix} S_{11}(i\omega) & S_{12}(i\omega) \\ S_{21}(i\omega) & S_{22}(i\omega) \end{bmatrix} \begin{bmatrix} H_1(i\omega) & H_2(i\omega) \end{bmatrix}^{*T} \tag{23}$$

The RMS value of the response parameter is related to the PSD function by

$$\sigma_{out} = \sqrt{\frac{1}{2\pi}\int_0^\infty S_{out}(\omega)d\omega} \tag{24}$$

The sensitivity of the PSD function of a response parameter to structural changes can be calculated by

$$\frac{\partial S_{out}}{\partial p} = 2Re\left(\frac{\partial}{\partial p}\begin{bmatrix} H_1 & H_2 \end{bmatrix}\begin{bmatrix} S_{11} & S_{12} \\ S_{21} & S_{22} \end{bmatrix}\begin{bmatrix} H_1 & H_2 \end{bmatrix}^{*T}\right) \tag{25}$$

where p represents any parametric change (component natural frequency or a structural link property in our cases). The sensitivity of the associated RMS value is obtained by the differentiation of Eq. (20),

$$\frac{\partial \sigma_{out}}{\partial p} = \frac{1}{4\pi\sigma_{out}}\int_0^\infty \frac{\partial S_{out}(\omega)}{\partial p}d\omega \tag{26}$$

5. Numerical Application

5.1 General

The numerical application is of random acceleration response at several points in a vehicle traveling on a rough road. Figure 1 shows the structural finite element model of an SUV-type vehicle. The model, the road conditions and the response points of interest were provided by General Motors. The model has 5,174 grid points interconnected by 5,654 elements with the total of 22,799 degrees of freedom. The structure is divided into 7 functional components, as described in Ref. [9]. For the purpose of method evaluation, some functional components were merged in the current work to form 3 components. The components are interconnected by 21 soft elements (of stiffness and/or damping) and 4 structural links, as detailed below.

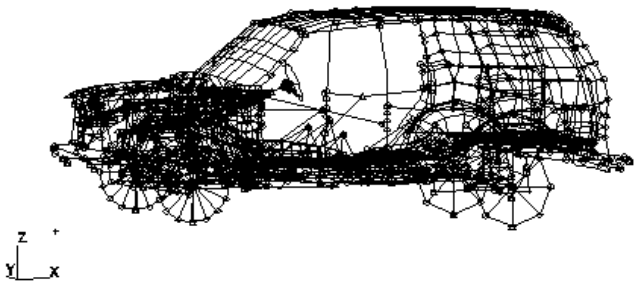

Figure 1: The vehicle finite-element model

The main purpose of the numerical application presented in this paper is to demonstrate the use of the fictitious-mass modal coupling technique to sensitivity analysis of random response with respect to changes in component natural frequencies and changes in the mechanical properties of structural connections between the different components. The benchmark problem, the modeling of the separate components, the modal coupling process, the random response analysis and the sensitivity analysis are described in the following subsections.

5.2 The Benchmark Problem

The vehicle model shown in Figure 1 is excited in the benchmark problem by enforced vertical accelerations due to a 37.5 mph travel on a rough road. The excitation is defined by power-spectral-density (PSD) functions associated with the accelerations in the Z direction at the bottom point of the four wheels shown in Figure 2. The PSD functions of the input accelerations are defined for the front wheels. The rear wheels are experiencing the same excitations as the respective front ones, but with a time delay of τ=0.177s.

Large masses of 10^6 tons each are introduced at the excitation points, in the Z direction. These large masses should not be confused with the interface fictitious masses described below. The application forces that are equal to the prescribed accelerations times the large added masses enforce the required excitation accelerations. The excitation points are restrained in all the other directions, which yields three pure rigid-body modes. The four large masses at the excitation points yield, in effect, four modes of zero or almost-zero frequency. All these 4 modes are referred to below as rigid-body modes.

The response points are shown in Figure 3, four at the seats and four at the wheel centers. The benchmark NASTRAN runs calculated frequency response and PSD of the accelerations at the response points in all directions, in the frequency range of 1-50 Hz. The reference computations were performed using Solution 111 of MSC/NASTRAN. The 2-column complex matrix $[H(i\omega)]$ of output frequency response values due to right and left excitations was calculated by solving Eq. (1) with the forces of Eq. (18) at the right and the left wheels separately. The response spectrum matrix was then calculated by Eq. (19).

5.3 Component modes

The benchmark vehicle was divided into three components for the purpose of subsequent dynamic solutions by modal coupling. The definition of the various components and the associated model information are given in Table 1.

The separate components were loaded with fictitious masses at the interface coordinates with neighboring components. The number of interconnection degrees of freedom between the various components, and the fictitious mass terms loading them, are detailed in Table 2. The off-diagonal numbers indicate the number of linear/angular interface degrees of freedom. The diagonal terms indicate the mass/moment-of-inertia values used uniformly at the borders of each component.

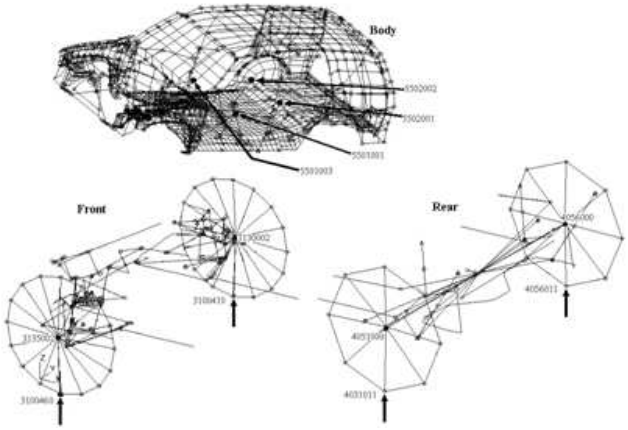

Figure 2: Excitation and output points

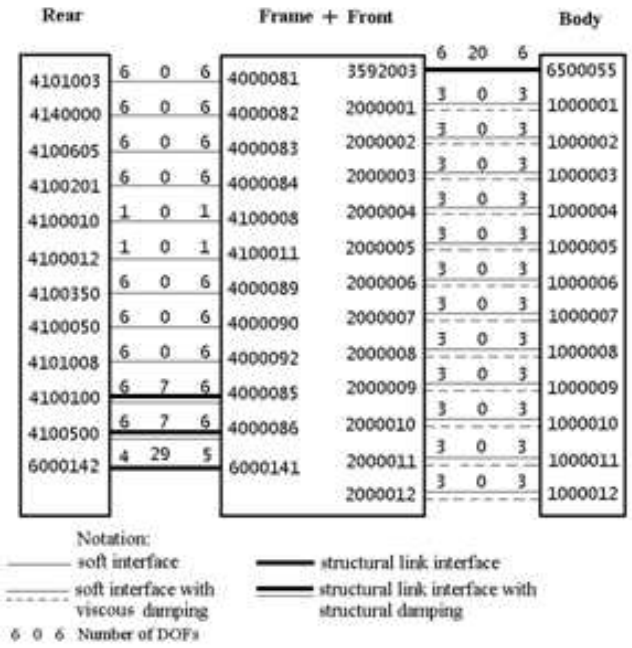

Figure 3: Interface points and interconnection elements

Component	Mass, kg	# of dof	# of grid points	# of elements
Body + Steering Column	963.9	18389	4014	2805
Frame + Front + Engine + Diff. Carrier	1070.0	4242	1038	1567
Rear	194.4	450	123	52
Total	2228.3	23081	5175	4424

Table 1: Components of the vehicle finite-element model

Component No.	1	2	3
1	250.0/0	39/3	
2	39/3	150.0/2.0*10^8	32/30
3		32/30	30.0/4.0*10^5

Table 2: Linear/angular fictitious mass terms (kg and $kg*mm^2$) and number of linear/angular interface coordinates (off-diagonal terms)

Table 3: Component modes taken into account

Component No.	Number of Modes	Highest Natural Frequency [Hz]
1	137	100.2
2	138	99.5
3	54	99.7

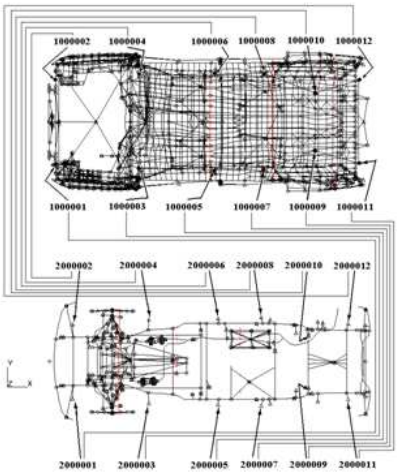

Figure 4: Interface points between Components 1 and 2

A summary of the interface points and the types of interconnection elements is given in Figure 3. There are two types of interconnection elements. "Soft" elements are simple springs, some of them with viscous damping, that have no inner degrees of freedom. "Structural Links" are structural interconnection components with inner degrees of freedom. Some of the elements of the structural links are assigned with structural damping. The interface points between Components 1 and 2 and between Components 2 and 3 are shown in Figures 4 and 5 respectively.

The number of modes taken from each component (including rigid-body modes) and the highest frequencies in the separate modal groups are given in Table 3. As will be shown later, these modes are sufficient for obtaining good results in the frequency range of interest, which was from 0 to 50Hz.

5.4 Normal modes by coupling

The mass and stiffness matrices of the coupled system were constructed as in Eq. (5), extended to include 3 components and 4 structural links. The number of degrees of freedom in the coupled system is the sum of the component modes taken into account, 329 as detailed in Table 3, plus 63 which is the number of inner coordinates of the structural links. The coupled 392*392 stiffness and mass matrices were used for calculating the lowest 91 natural frequencies below 50 Hz and the associated eigenvectors using Matlab. The 44 lowest frequencies

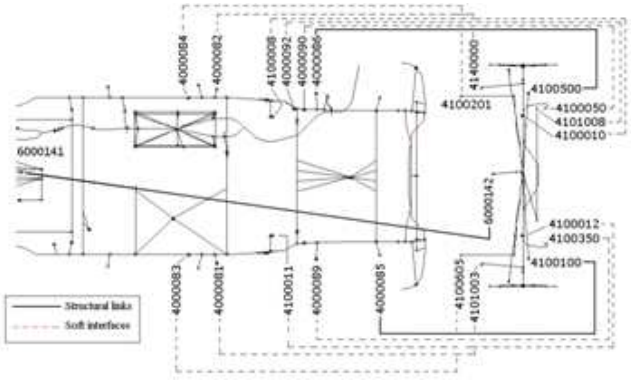

Figure 5: Interface points between Components 2 and 3

Mode	Frequency [Hz]	Direct [Hz]	Error [%]	Mode	Frequency [Hz]	Direct [Hz]	Error [%]
1	1.27	1.27	0.02	23	12.96	12.96	0.01
2	1.49	1.49	0.01	24	13.10	13.10	0.01
3	1.60	1.60	0.00	25	13.37	13.37	0.02
4	2.18	2.18	0.00	26	13.75	13.75	0.01
5	2.99	2.99	0.01	27	14.38	14.38	0.03
6	3.31	3.31	0.01	28	15.39	15.39	0.06
7	3.67	3.67	0.09	29	15.71	15.70	0.02
8	4.70	4.70	0.02	30	16.42	16.41	0.09
9	4.84	4.84	0.01	31	17.02	17.01	0.02
10	5.65	5.65	0.00	32	17.51	17.49	0.12
11	6.00	6.00	0.01	33	18.13	18.12	0.07
12	8.38	8.38	0.01	34	18.76	18.75	0.07
13	8.74	8.74	0.01	35	19.74	19.72	0.11
14	9.11	9.11	0.01	36	20.50	20.46	0.19
15	9.54	9.54	0.00	37	21.60	21.56	0.19
16	9.57	9.57	0.03	38	21.62	21.60	0.11
17	10.00	10.00	0.02	39	22.57	22.55	0.10
18	10.60	10.59	0.00	40	24.49	24.48	0.04
19	10.63	10.63	0.00	41	25.25	25.16	0.32
20	12.42	12.42	0.01	42	25.82	25.73	0.33
21	12.63	12.63	0.00	43	26.19	26.13	0.26
22	12.76	12.76	0.02	44	27.11	27.21	0.37

Table 4: Natural frequencies of the vehicle by coupling and by direct solution

(except for the 4 rigid-body zero frequencies) are compared to those obtained by direct MSC/NASTRAN solution in Table 4. It can be seen that the coupling procedure predicts the 44 frequencies below 26.2 *Hz* with frequency errors of less than 0.34%. The entire 91 frequencies below 50 *Hz* were calculated with frequency errors of less than 1.4%. The accuracy of the resulting modes will be examined by the accuracy of the dynamic response calculations in the following sections.

The component modes that were generated with boundary fictitious masses were also used for calculating the free-free separate component modes without the fictitious masses. The purpose of this "cleaning" is to examine the adequacy of the modal coupling procedure for sensitivity analysis with variations in the structural properties of the interconnection elements. An accurate cleaning process would also indicate that sensitivities with respect to natural frequencies of components with fictitious masses other than those used for modal coupling, as discussed after Eq. (16), are feasible. As shown in Ref. [9], the eigenvalues of Component A, for example, without the boundary fictitious masses are those associated with the free undamped equation of motion

$$\left[M_A - \phi_{IA}^T M_{FA} \phi_{IA}\right] \left\{\ddot{\xi}_A\right\} + \left[\Omega_A M_A\right] \left\{\xi_A\right\} = \{0\} \tag{27}$$

All the component frequencies up to $50Hz$ obtained by eigensolution of Eq. (23) were up to 1% larger than the corresponding frequencies obtained directly from the finite-element model.

5.5 Dynamic response to random excitation by modal coupling

The benchmark problem was calculated by modal coupling using Eq. (1) with the stiffness and mass matrices of Eq. (5), the damping and structural damping matrices of Eq. (8), and the excitation vector of Eq. (9), all expanded to include the 3 components and 3 structural links. The modal transformation of Eq. (10) was also used and the problem size was reduced to the 91 lowest-frequency

Table 5: Maximal PSD responses [$mm^2/s^4/Hz$] by coupling and by direct calculations.

Grid Point	Direct	Freq. [Hz]	Maximum of Acceleration PSD		Error [%]
			Modal Coupling	Direct	
3130002	X	1.3	1.7709	1.7742	0.183
	Y	1.5	15.724	15.732	0.056
	Z	1.4	5.3247	5.3206	-0.08
3135002	X	1.3	1.6464	1.6494	0.181
	Y	1.5	16.937	16.952	0.084
	Z	1.4	6.1185	6.1141	-0.072
4051000	X	2.2	2.8713	2.8782	0.241
	Y	1.5	13.453	13.468	0.113
	Z	1.5	7.0416	7.0452	0.05
4056000	X	2.2	2.076	2.0759	-0.008
	Y	1.5	13.453	13.468	0.113
	Z	1.5	3.3872	3.3854	-0.051
5501001	X	1.3	8.2532	8.2597	0.078
	Y	1.5	46.512	46.576	0.138
	Z	1.5	45.302	45.333	0.069
5501003	X	1.3	7.4875	7.4921	0.062
	Y	1.5	47.389	47.455	0.140
	Z	1.5	18.118	18.117	-0.007
5502001	X	1.3	9.3799	9.3858	0.063
	Y	1.5	54.740	54.819	0.143
	Z	1.5	19.695	19.718	0.114
5502002	X	1.3	8.733	8.7388	0.063
	Y	1.5	54.390	54.468	0.143
	Z	1.6	8.9571	8.9729	0.175

modes, as done in the benchmark case of Ref. [9]. The resulting PSD curves at the 8 output points in the X, Y and Z directions, calculated by Eq. (19), were compared in Ref. [9] to those obtained directly by MSC/NASTRAN with the full vehicle model. It was shown that the results obtained by the two methods are practically identical. The numerical peak values that are compared in Table 5 exhibit insignificant differences as well. The RMS values of the response parameters are compared to those obtained directly by MSC/NASTRAN in Table 6, exhibiting negligible differences.

5.6 Sensitivity of dynamic response to structural changes

Derivatives of the RMS values of the selected response parameters were calculated with respect to changes in structural links and changes in component natural frequencies. Direct analytical derivatives were based on Eqs. (21) and (22). Finite-difference derivatives were calculated for comparison by repeating the response calculations with parameter variations of 0.1% of their original values. Comparisons between the direct and finite-difference RMS derivative with respect to stiffness and damping values in the Y direction of the soft element connecting point 1000003 in Component A to point 2000003 in Component B are given in Tables 7 and 8. The analytical derivatives in Table 7 are very accurate. The derivatives w.r.t. damping in Table 8 are also of good percentage accuracy (errors of less than 2%), except for points of very small derivatives. Comparisons between the direct and finite-difference RMS derivative with respect to a damping value in the Z direction of the structural link connecting point 4000085 in Component B to point 4100100 in Component C are given in Tables 9. All percentage errors here are below 0.4%, except for a single point of a very small derivative, point 5502001 in Z direction.

Sensitivities of the RMS response values to changes in component lowest

Output Grid Point	Direction	σ_{out}, mm /s^2 Modal coupling	σ_{out}, mm /s^2 Direct	Error [%]
3130002	X	0.62	0.62	-0.06
3130002	Y	1.12	1.12	-0.06
3130002	Z	2.17	2.17	-0.04
3135002	X	0.45	0.45	-0.18
3135002	Y	1.11	1.12	-0.06
3135002	Z	2.24	2.24	-0.01
4051000	X	0.89	0.89	-0.34
4051000	Y	1.85	1.86	-0.08
4051000	Z	2.52	2.52	0.04
4056000	X	0.70	0.70	-0.11
4056000	Y	1.85	1.86	-0.08
4056000	Z	2.37	2.37	0.09
5501001	X	0.88	0.88	-0.09
5501001	Y	1.19	1.19	-0.03
5501001	Z	1.42	1.42	-0.04
5501003	X	0.67	0.67	-0.08
5501003	Y	1.22	1.22	-0.03
5501003	Z	1.33	1.33	-0.02
5502001	X	0.88	0.88	-0.61
5502001	Y	1.75	1.75	-0.09
5502001	Z	1.23	1.23	-0.06
5502002	X	0.72	0.72	-0.28
5502002	Y	1.76	1.76	-0.09
5502002	Z	1.28	1.28	-0.05

Table 6: RMS response values by coupling and by direct calculations.

non-zero natural frequencies with fictitious masses are shown in Table 10 for Component A, Table 11 for Component B and Table 12 for Component C. One can learn from these tables on the relative effects of the various component frequencies on system-level response. It can be observed is our case that the analyzed frequency deviations in component B have larger effect than the analyzed deviation in other components, and that a change in the frequency of Mode 3 in Component B has the largest effect on the vertical response of the driver's seat (point 5501001). These are examples of sensitivity information that may be of interest in the design process.

6. Conclusion

The fictitious-mass modal coupling approach facilitates convenient and efficient evaluation of the sensitivity of system-level performance to parametric changes in sub-system structural properties. The fictitious masses that load the sub-system interface coordinates yield high-accuracy system-level dynamic response properties and their sensitivity to parametric changes without updating the modal coordinates. The resulting new modeling procedure facilitates the performance of extensive high-accuracy parametric design sessions in an on-line manner using common utility software packages such as Matlab, without returning to the finite-element model. Such sensitivities may be of high importance in defining design criteria and acceptance procedures, and during the vehicle design process itself. The small size of the computational model facilitates its efficient inclusion is automatic design optimization schemes with system-level behavior constraints. The techniques developed in this study have the potential to improve the computational accuracy and efficiency of the vehicle finite-element model in predicting the effects of subsystem structural accuracy requirements on system-level vehicle vibrations.

Table 7: Derivatives of RMS response values with respect to changes in a stiffness element connecting Components A and B.

Output Grid Point	Direction	Derivative $\times 10^{-6}$	Finite Difference Derivative $\times 10^{-6}$	Error [%]
3130002	X	-0.78	-0.78	0.06
3130002	Y	-1.95	-1.95	0.04
3130002	Z	0.20	0.20	0.03
3135002	X	0.09	0.09	-0.10
3135002	Y	-1.60	-1.60	0.05
3135002	Z	0.22	0.22	0.06
4051000	X	-2.91	-2.91	0.05
4051000	Y	-4.04	-4.04	0.04
4051000	Z	-0.37	-0.37	0.05
4056000	X	-2.62	-2.62	0.05
4056000	Y	-4.04	-4.04	0.04
4056000	Z	0.09	0.09	0.04
5501001	X	-1.57	-1.57	0.05
5501001	Y	-0.12	-0.12	-0.17
5501001	Z	0.05	0.05	0.04
5501003	X	-1.26	-1.26	0.03
5501003	Y	-0.06	-0.06	-0.32
5501003	Z	-0.21	-0.21	-0.16
5502001	X	-1.40	-1.40	0.01
5502001	Y	-2.45	-2.44	0.04
5502001	Z	-0.02	-0.02	0.25
5502002	X	-0.73	-0.73	0.01
5502002	Y	-2.47	-2.47	0.04
5502002	Z	-0.06	-0.06	-0.65

Table 8: Derivatives of RMS response values with respect to changes in a damping element connecting Components A and B.

Output Grid Point	Direction	Derivative $\times 10^{-5}$	Finite Difference Derivative $\times 10^{-5}$	Error [%]
3130002	X	-0.79	-0.79	0.04
3130002	Y	-3.90	-3.92	-0.52
3130002	Z	-0.01	-0.01	9.12
3135002	X	-1.55	-1.54	0.07
3135002	Y	-5.22	-5.24	-0.46
3135002	Z	-3.81	-3.81	0.00
4051000	X	-0.08	-0.10	-25.6
4051000	Y	-0.86	-0.90	4.94
4051000	Z	-2.17	-2.18	-0.11
4056000	X	-1.93	-1.95	-1.39
4056000	Y	-0.86	-0.90	-4.94
4056000	Z	-0.39	-0.39	-1.05
5501001	X	-0.23	-0.24	-3.90
5501001	Y	-1.60	-1.60	-0.19
5501001	Z	-2.72	-2.72	-0.21
5501003	X	-6.73	-6.75	-0.23
5501003	Y	-0.20	-0.20	-2.04
5501003	Z	-0.50	-0.52	-2.92
5502001	X	-23.70	-23.70	-0.01
5502001	Y	-1.35	-1.37	-1.95
5502001	Z	-5.28	-5.28	-0.04
5502002	X	-9.22	-9.23	-0.13
5502002	Y	-1.62	-1.64	-1.61
5502002	Z	-4.98	-4.99	-0.25

Output Grid Point	Direction	Derivative $\times 10^{-2}$	Finite Difference Derivative $\times 10^{-2}$	Error [%]
3130002	X	-3.05	-3.05	0.03
3130002	Y	-6.38	-6.38	0.02
3130002	Z	-0.80	-0.80	0.00
3135002	X	-1.78	-1.78	0.02
3135002	Y	-5.86	-5.86	0.02
3135002	Z	0.11	0.11	0.05
4051000	X	0.64	0.64	-0.02
4051000	Y	-2.69	-2.69	0.04
4051000	Z	-9.93	-9.93	0.06
4056000	X	-0.25	-0.25	0.13
4056000	Y	-2.69	-2.69	0.04
4056000	Z	-20.14	-20.13	0.04
5501001	X	0.47	0.47	0.00
5501001	Y	-1.64	-1.64	0.04
5501001	Z	0.28	0.28	-0.33
5501003	X	-0.44	-0.44	0.00
5501003	Y	-1.48	-1.47	0.04
5501003	Z	-1.20	-1.20	0.10
5502001	X	-4.71	-4.71	0.04
5502001	Y	0.18	0.18	-0.26
5502001	Z	0.01	0.01	-9.70
5502002	X	-2.03	-2.03	0.03
5502002	Y	0.42	0.42	-0.11
5502002	Z	-1.57	-1.56	0.06

Table 9: Derivatives of RMS response values with respect to changes in a damping element connecting Components B and C.

Output Grid Point	Direction	Derivative at f=1.1073 Hz, $(mm/s^2)/Hz \times 10^{-5}$	Derivative at f=1.1349 Hz, $(mm/s^2)/Hz \times 10^{-5}$
3130002	X	-15.53	-4.08
3130002	Y	75.23	2.40
3130002	Z	6.83	-0.87
3135002	X	9.04	0.80
3135002	Y	88.31	1.88
3135002	Z	-9.16	-3.97
4051000	X	-13.44	-3.20
4051000	Y	7.82	-0.20
4051000	Z	5.19	0.39
4056000	X	9.39	0.86
4056000	Y	7.82	-0.20
4056000	Z	0.09	4.16
5501001	X	-32.61	-0.96
5501001	Y	35.72	-0.05
5501001	Z	-57.63	-12.64
5501003	X	-45.09	-3.30
5501003	Y	16.57	-2.19
5501003	Z	3.78	-3.51
5502001	X	-182.06	-124.93
5502001	Y	-1.15	-7.25
5502001	Z	-75.25	-24.37
5502002	X	-39.02	-35.91
5502002	Y	-6.01	-8.09
5502002	Z	1.84	-14.47

Table 10: Derivatives of RMS response values with respect to frequency changes in Component A

Table 11: Derivatives of RMS response values with respect to frequency changes in Component B

Output Grid Point	Direction	Derivative at f=0.4414 Hz, $(mm/s^2)/Hz \times 10^{-2}$	Derivative at f=0.7229 Hz, $(mm/s^2)/Hz \times 10^{-2}$
3130002	X	-33.10	72.14
3130002	Y	7.95	-34.43
3130002	Z	-0.27	-12.30
3135002	X	-31.55	80.32
3135002	Y	5.90	-32.69
3135002	Z	-5.86	0.00
4051000	X	-20.10	-22.58
4051000	Y	11.66	95.12
4051000	Z	-6.36	8.53
4056000	X	-16.86	-6.35
4056000	Y	11.66	95.12
4056000	Z	-3.25	-1.10
5501001	X	-8.63	-12.09
5501001	Y	1.61	56.13
5501001	Z	19.01	2.79
5501003	X	-5.91	-1.53
5501003	Y	1.69	61.07
5501003	Z	28.25	19.23
5502001	X	1.86	-13.63
5502001	Y	-17.06	80.15
5502001	Z	6.94	-4.08
5502002	X	-1.73	-3.24
5502002	Y	-18.67	80.48
5502002	Z	13.31	6.04

Table 12: Derivatives of RMS response values with respect to frequency changes in Component C

Output Grid Point	Direction	Derivative at f=0.3332 Hz, $(mm/s^2)/Hz \times 10^{-5}$	Derivative at f=0.4769 Hz, $(mm/s^2)/Hz \times 10^{-5}$
3130002	X	-27.52	-223.34
3130002	Y	-42.34	-84.30
3130002	Z	-43.02	-16.62
3135002	X	-54.95	-156.62
3135002	Y	-21.11	30.33
3135002	Z	-8.98	-17.13
4051000	X	9.42	-152.96
4051000	Y	60.27	-920.07
4051000	Z	-44.72	-58.50
4056000	X	-24.00	-70.02
4056000	Y	60.27	-920.07
4056000	Z	-107.27	-64.70
5501001	X	-36.81	-72.09
5501001	Y	2.74	-516.43
5501001	Z	148.78	-182.37
5501003	X	-217.03	-6.00
5501003	Y	14.78	-541.66
5501003	Z	29.62	-407.68
5502001	X	-283.60	-39.22
5502001	Y	48.02	-760.83
5502001	Z	-46.92	-30.66
5502002	X	-299.52	-4.33
5502002	Y	52.96	-746.44
5502002	Z	-431.46	-260.51

7. Acknowledgements

The authors wish to acknowledge the GM Noise & Vibration Center for providing the vehicle finite element model and the GM Research & Development Center, especially R. V. Lust and D. J. Nefske, for their support and technical contributions. This work was also supported by the Centre for Absorption in Science of the Ministry of Immigrant Absorption and the Committee for Planning and Budgeting of the Council for Higher Education under the framework of the KAMEA Program.

8. References

1 R.R.Craig, Coupling of Substuctures for Dynamic Analyses: An Overview, Proceedings of the 41^{st} Structures, Structural Dynamics and Materials Conference, AIAA Paper AIAA-2000-1573, April 2000.

2 W.C.Hurty, Dynamic Analysis of Structural Systems by Component Modes, AIAA Journal, Vol. 3, No. 4, 1965, pp. 678-685.

3 R.R.Craig and M.C.C.Bampton., Coupling of Substructures for Dynamic Analyses, AIAA Journal, Vol. 6, No. 7, 1968, pp. 1313-1319.

4 R.L.Goldman, Vibration Analysis by Dynamic Partitioning, AIAA Journal, Vol. 7, No. 6 1969, pp. 1152-1154.

5 S.N.Hou, Review of Modal Synthesis Techniques and a New Approach, Shock and Vibration Bulletin, Vol. 40, Pt. 4, Dec. 1969, pp. 25-30.

6 W.A.Benfield and R.F.Hruda, Vibration Analysis of Structures by Component Mode Substitution, AIAA Journal, Vol. 9, No. 7 1971, pp. 1255-1261.

7 R.H.MacNeal, A Hybrid Method of Component Mode Synthesis, J. Computers and Structures, Vol. 1, No. 4, Dec. 1971, pp. 581-601.

8 S.Rubin, Improved Component-Mode Representation in Structural Dynamic Analysis', AIAA Journal, Vol. 13, No. 8, 1975, pp. 995-1006.

9 M.Karpel, B.Moulin, V.Feldgun, Component Mode Synthesis of a Vehicle System Model Using the Fictitious Mass Method. Journal of Vibration and Acoustics, Vol. 129, No. 1, 2007, pp. 72-83.

10 M.Karpel, D.Raveh, Fictitious Mass Element in Structural Dynamics. *AIAA Journal*, Vol. 34, No. 3, 1996, pp. 607-613.

11 M.Karpel, M.Newman, Accelerated Convergence for Vibration Modes Using the Substructure Coupling Method and Fictitious Coupling Masses. *placecountry-regionIsrael Journal of Technology*, Vol.13, 1975, pp. 55-62.

12 M.Karpel, Efficient Vibration Mode Analysis of Aircraft with Multiple External Store Configurations. *Journal of Aircraft*, Vol. 25, No. 8, 1988, pp. 747-751.

13 M.Karpel, D.Raveh, S.Ricci, Ground Vibration Tests of Space-Structure Components Using Boundary Masses. *Journal of Spacecraft and Rockets*, Vol. 33, No. 2, 1996, pp. 272-277.

14 M.Karpel, S.Ricci, Experimental Modal Analysis of Large Structures by Substructuring. *Mechanical Systems and Signal Processing*, Vol. 11, No. 2, 1997, pp. 245-256.